J. Plant Production, Mansoura Univ., Vol. 6 (12):1917-1940,2015

SPECTRAL SIGNATURE IDENTIFICATION AND SURFACE AREA ESTIMATION FOR FRUIT CROPS GROWN IN TIBA REGION OF WESTERN NILE DELTA OF EGYPT BY USING LANDSAT-8 SATELLITE REMOTE SENSING DATA

El-Ansary, D. O.

Precision Agriculture Laboratory, Department of Pomology, Faculty of Agriculture (El-Shatby), University of Alexandria, 21545, Egypt

Corresponding author e-mail: diaa.elansary@alexu.edu.eg / diaaagri@hotmail.com / Tel.: +02-01000150804

ABSTRACT

In this research, satellite remote sensing data and field measured ground-truth data were used to identify the spectral signature and estimate the total surface area for fruit crops grown in Tiba region of western Nile delta of Egypt. Global position system (GPS) data collection and surface bare soil sampling for this research was conducted in Tiba region during 2012 and 2013 seasons. Ground-truth data included: eleven fruit crops: orange, mandarin, lime & lemon, grape, apple, peach, apricot, plum, guava, mango, and cactus pear; six other crops: tomato, squash, wheat, berseem clover, broad bean, and sugarbeet; and finally bare soil. One Landsat-8 Operational Land Imager (OLI) and Thermal Infrared Sensor (TIRS) satellite image for the study area covering WRS-path 177 and WRS-row 39, acquired on 19 March 2013 was radiometric calibrated to top of atmospheric reflectance and spectral signature curves were developed for each crop and for grouped crops against bare soil. Nine vegetation indices (VIs) were derived from the reflectance wavelength of the visible, near infrared and shortwave infrared parts of spectrum and included: Normalized Difference Vegetation Index (NDVI), Ratio Vegetation Index (RVI), Transformed Vegetation Index (TVI), Ashburn Vegetation Index (AVI), Soil-Adjusted Vegetation Index (SAVI), Modified Soil-Adjusted Vegetation Index 2 (MSAVI2), Tasseled Cap Brightness (TCB), Tasseled Cap Greenness (TCG), and Tasseled Cap Wetness (TCW). Supervised classifications for band reflectance and VIs were performed to estimate areas of fruit crops, other crops and bare soil, and accuracy assessment for the developed research methodology was presented. Moreover, multiple linear regression modeling (MLRM) equations to predict bare soil calcium carbonate (CC) %, electrical conductivity (EC) in $dS \cdot m^{-1}$, pH, and soil texture (sand, silt, and clay %) by using the first eight bands of Landsat-8 OLI remote sensing data of bare soil as regressors were also developed, and soil mapping units (SMU) in Tiba were presented by using geographic information system (GIS) interpolated maps. Results indicated that satellite band reflectance estimates for cropping pattern were more precise than VIs, and it is recommend to use reflectance of band 3 (0.53 – 0.59 µm) or 4 (0.64 – 0.67 µm) to estimate surface area for fruit crops. MLRM prediction indicated that in most Tiba region CC, EC, and SMU of bare soil were predicted with high accuracy.

Keywords: Remote sensing, Landsat-8, spectral signature, vegetation indices, cropping pattern, fruit crops, soil mapping units

INTRODUCTION

Nowadays, the world horticultural industry is experiencing a massive change in how to manage and deal with agricultural information. There is an increasing applications in using satellite remote sensing imagery as means for accurate mapping and monitoring of spatial and temporal spectral signature of cropping patterns (Reis and Tasdemir, 2011; Kolios and Stylios, 2013; Maeda *et al*., 2014; and Qin *et al*., 2015), detecting crop physiological status (Othman *et al*., 2014), identifying irrigation water scarcity problems (Serra and Pons, 2013), monitoring crop evapotranspiration for irrigation management (González-Dugo *et al*., 2013 and Mateos *et al*., 2013), and estimating fruit crop yield (Maselli *et al*., 2012) and losses (Tapia-Silva *et al*., 2011). Ongoing agricultural activities including changing cropping patterns and technical operations such as irrigation, fertilization, and chemical applications lead to changes in soil health and fertility and therefore soil productivity (Paudel *et al*., 2015). Variable soil characteristics in the field influence, growth, yield of crops, and affect the incidence of pests (Patzold *et al*., 2008). Identifying and mapping crops is important for agriculture and economic national departments and agencies to prepare an inventory of what was grown and when and prepare the future action plans (Shrivastava and Gebelein, 2007). Traditional methods to collect these information are census and ground surveying, which have several limitation including contradiction, time and energy consumption, and difficulties to reach on time, whereas, remote sensing offers a new standardized alternative method, which offers a fast synoptic view of agricultural regions, efficient, reliable, and can provide early forecasting for production and for future planning.

Landsat-1 satellite was first launched 1972, and was followed by a series of Landsat 2 to 7, and finally landsat-8 Operational Land Imager (OLI) and Thermal Infrared Sensor (TIRS) launched on February 11th 2013, which provided the longest continuous recorded history for entire globe. Landsat-8 satellite has a 16 day repeat cycle, data are segmented into 185 × 180 km scenes, has a medium spatial resolution, and the archive is freely available via the internet (Roy *et al*., 2014). Integration of technologies such as global positioning systems (GPS), geographic information systems (GIS), and remote sensing (RS) data are making it possible to identify and map the variability within a field, and by providing information about where variability occurs, it is possible to improve plant management practices and increase yield and quality of crop (Heiniger, 1999 and Reynolds & Rezaei, 2014). Spectral signature is a characteristics for a crop or soil for their interaction with the solar radiation energy by either absorption, reflection, or scattering patterns (Papes *et al*., 2013), and this interaction may vary according to crop species, phenological stage, and sampling data (Lopez-Granados *et al*., 2010).

The target area in this study is Tiba region located in western Nile delta of Egypt. It is a newly reclaimed area characterized by arid climatic conditions with very limited rainfall. Tiba region soil is sandy with very limited water holding capacity. Agricultural production includes fruits, vegetables and field

crops, and this cropping pattern is changing regularly according to market demands and agricultural production challenges with a progressive shifting toward fruit crop cultivation. Irrigation is practiced by using Nile water (Branch 20), which is applied by drip (for fruits and vegetables) and sprinkler (for field crops) irrigation systems. Tiba region was chosen for this research as it represents the desert rural reclamation projects targeting settlement of small-scale farmers started in late 1980s and early 1990s, the potential for high value fruit crop production for exports, and its environment vulnerability due to current undesirable environmental impacts and production problems. The objectives of this study were to use remote sensing data coupled with GPS and GIS to identify the spectral signature of fruit crops, estimate the total surface area grown with fruit crops, and predict bare soil characterization and main soil mapping units in Tiba region. The results of this study will enable further advances in research studies regarding soil and crop productivity, crop health monitoring, and site-specific crop management by remote sensing imagery.

MATERIALS AND METHODS

- **Study location, ground-truth data collection, bare soil sampling and laboratory analysis:**

Sampling and data collection of this research was conducted in Tiba region of western Nile delta of Egypt (west Nubaria) during 2012 and 2013 seasons. Figure (1) illustrate the location of Tiba region in western Nile delta of Egypt, and Figure (2) shows the composite (blue, green and red bands) Landsate-8 satellite image of Tiba region. Field visits were conducted to locate the ground-truth points by a global positioning system (GPS) instrument [Garmin GPSmap 62s, Taiwan]. Decision of sample location for crops and soil was based on field observation to cover all possible visual variabilities. Starting from March 2012 until March 2013, fruit crop farm locations were collected. Other Crops including vegetables and field crops were collected from November 2012 till March 2013. Figure 3 illustrates the GPS locations and number of ground-truth sites for each crop type and bare soil in Tiba region. Data of all varieties/cultivars for each crop type were collected and pooled together for analysis. The crop type's description and bare soil samples were: (1) Fruit crops: orange [*Citrus sinensis* (L.) Osbeck], mandarin [*Citrus reticulata*; *C. unshiu*; *C. clementina*], lime [*Citrus aurantifolia* (Christm.) Swingle] & lemon [*Citrus limon* (L.) Osbeck], grape [*Vitis vinifera* L.], apple [*Malus domestica* Borkh], peach [*Prunus persica* (L.) Batsch], apricot [*Prunus armeniaca* L.], plum [*Prunus salicina* L.], guava [*Psidium guajava* L.], mango [*Mangifera indica* L.], and cactus pear [*Opuntia ficus-indica* L.]; (2) Other crops: tomato [*Lycopersicon esculentum* Mill.], squash [*Cucurbita pepo* L.], wheat [*Triticum aestivum* L.], berseem (Egyptian) clover [*Trifolium alexandrinum* L.], broad bean [*Vicia faba* L.], and sugarbeet [*Beta vulgaris* L.]; and (3) Bare soil: a five cm depth representative bare soil samples were collected from 54 ground-truth locations during the period from

January 2013 to March 2013. Soil samples were air dried, gently ground, and sieved through a 2 mm sieve to separate the gravel fraction. Soil texture for fractions less than 2 mm was determined by the Hydrometer method (Black *et al*., 1965). Electrical conductivity [EC ($dS \cdot m^{-1}$)] and pH of bare soil samples were measured in solution extracts at 25°C by using the saturated soil paste method (Richards, 1954) by EC- and pH-meters. Measurement of total calcium carbonate [CC (%)] was made by a calcimeter apparatus (Black *et al*., 1965). Samples and data analysis were conducted at Precision Agricultural Laboratory (PAL), Department of Pomology, Faculty of Agriculture (El-Shatby), University of Alexandria, Egypt.

- **Satellite remotes sensing data:**

One Landsat-8 Operational Land Imager (OLI) and Thermal Infrared Sensor (TIRS) satellite image courtesy of the U.S. Geological Survey (USGS) for the study area covering WRS-path 177 and WRS-row 39, acquired on 19 March 2013, center time = 08:30:42.69, image quality OLI = 9, and cloud cover = 2.02, was used in this study. The spectral ranges and resolutions form band 1 to band 8 which was used for the analysis in this study data are as following (Roy *et al*., 2014): Band 1 (Blue 1): 0.43 – 0.45 µm, 30 m resolution; Band 2 (Blue 2): 0.45 – 0.51 µm, 30 m resolution; Band 3 (Green): 0.53 – 0.59 µm, 30 m resolution; Band 4 (Red (RED)): 0.64 – 0.67 µm, 30 m resolution; Band 5 (Near infrared (NIR)): 0.85 – 0.88 µm, 30 m resolution; Band 6 (Shortwave infrared 1 (SWIR1)): 1.57 – 1.65 µm, 30 m resolution; Band 7 (Shortwave infrared 2 (SWIR2)): 2.11 – 2.29 µm, 30 m resolution; Band 8 (Panchromatic): 0.50 – 0.68 µm, 15 m resolution.

- **Geographic information systems (GIS) and satellite image processing:**

All procedures of GIS and image radiometric calibration were performed by using ESRI ArcGIS Version 10.0 Software package. The image was projected to the Universal Transverse Mercator (UTM), with a spheroid and datum of WGS 84 and Zone N35. A subset images were extracted according to ArcGIS procedures from the original final processed image bands and were used for vegetation indices (VIs) calculations and the supervised classifications for bands and VIs. Corresponding reflectance and VIs values were extracted from the subset image of bands and VIs for each ground-truth location, and data were subject to descriptive and Post-Hoc statistical analysis.

- **Remote Sensing Calculations:**

A) Conversion of Landsat-8 OLI band digital number (DN) to top of atmosphere (TOA) reflectance was done in two steps (Chander *et al*., 2009):

1- Conversion of digital number to at-sensor spectral radiance:

$$L_\lambda = \left(\frac{LMAX_\lambda - LMIN_\lambda}{Q_{calmax} - Q_{calmin}}\right)(Q_{cal} - Q_{calmin}) + LMIN_\lambda$$

Where

L_λ = Spectral radiance at the sensor's aperture [$W/(m^2\ sr\ \mu m)$]

Q_{cal} = Quantized calibrated pixel value [DN]

Q_{calmin} = Minimum quantized calibrated pixel value corresponding to $LMIN_\lambda$ [DN]

Q_{calmax} = Maximum quantized calibrated pixel value corresponding to $LMAX_\lambda$ [DN]

$LMIN_\lambda$ = Spectral at-sensor radiance that is scaled to Qcalmin [W/(m^2 sr µm)]
$LMAX_\lambda$= Spectral at-sensor radiance that is scaled to Qcalmax [W/(m^2 sr µm)]

2-Conversion of at-sensor spectral radiance to TOA reflectance:

$$\rho_\lambda = \frac{\pi \cdot L_\lambda \cdot d^2}{ESUN_\lambda \cdot \cos\theta_s}$$

Where
ρ_λ= Planetary TOA reflectance [unitless]
π = Mathematical constant equal to ~3.14159 [unitless]
L_λ= Spectral radiance at the sensor's aperture [W/(m^2 sr µm)]
d = Earth–Sun distance [astronomical units]
$ESUN_\lambda$= Mean exoatmospheric solar irradiance [W/(m^2 µm)]
$\cos\theta_s$= Solar zenith angle [degrees]

B) Calculation of vegetation indices (VI) from TOA reflectance: Nine types of VIs were used

1- Normalized Difference Vegetation Index (NDVI): (Rhew *et al*., 2011)

$$NDVI = \frac{(NIR - RED)}{(NIR + RED)}$$

2- Ratio Vegetation Index (RVI): (Richardson & Wiegand, 1977)

$$RVI = \frac{Red}{NIR}$$

3- Transformed Vegetation Index (TVI): (Tucker, 1979)

$$TVI = \sqrt{\left(\frac{NIR - RED}{NIR + RED}\right) + 0.5}$$

4- Ashburn Vegetation Index (AVI): (Perry & Lautenschlager, 1984)

$$AVI = 2\,NIR - RED$$

5- Soil-Adjusted Vegetation Index (SAVI): (Jiang *et al*., 2006)

$$SAVI = \frac{NIR - RED}{NIR + RED + L}(1 + L)$$

6- Modified Soil-Adjusted Vegetation Index 2 (MSAVI2): (Laosuwan & Uttaruk, 2014)

$$MSAVI2 = \frac{(2NIR + 1) - \sqrt{(2NIR + 1)^2 - 8(NIR - RED)}}{2}$$

7- Tasseled Cap Brightness (TCB): (Baig *et al*., 2014)

$$TCB = 0.3029\,Blue2 + 0.2786\,Green + 0.4733\,RED + 0.5599\,NIR + 0.508\,SWIR1 + 0.1872\,SWIR2$$

8- Tasseled Cap Greenness (TCG): (Baig *et al*., 2014)

$$TCG = -0.2941\,Blue2 - 0.243\,Green - 0.5424\,RED + 0.7276\,NIR + 0.0713\,SWIR1 - 0.1608\,SWIR2$$

9- Tasseled Cap Wetness (TCW): (Baig *et al*., 2014)

$$TCW = 0.1511\,Blue2 + 0.1973\,Green + 0.3283\,RED + 0.3407\,NIR - 0.7117\,SWIR1 - 0.4559\,SWIR2$$

Where
Blue2, Green, RED, NIR, SWIR1, SWIR2, are corresponding band wavelength TOA reflectance
L = Soil adjustment factor (L = 0.5)

- **Statistical Analysis:**

All extracted data were subject to statistical analysis by using IBM SPSS Statistics Version 21 software package as following:

1-Reflectance and VIs extracted data from processed images: A univariate general linear model was used to analyze the data and a Post-Hoc Tukey test was applied to examine differences among data groups. Significance was determined at P-value < 0.05. As there were no significant differences among individual crops and bare soil due to high standard deviation of values from mean values at each band and VI (data not shown), each group of data for fruit crops, other crops, and bare soil were pooled together and a significant differences were obtained among groups for all bands, except band 5, and for all VIs.

2-Bare soil characterization prediction model: A multiple linear regression analysis by the enter regression method was performed to predict soil texture (sand, silt, and clay), EC, pH and CC by using extracted reflectance data of band 1 to band 8 as repressors. Effect size (R^2) values was presented and significance was determined at P-value < 0.01.

- **Supervised classification for bands and VIs:**

Supervised classifications for all bands and VIs which had significant separation among all groups by the Post-Hoc test were performed by using the mean ± standard deviation (SD) values as minimum and maximum clustering borders around the mean value. As there was an overlapping for the standard deviation values of other crops with values of both fruit crops and bare soil (Table 1), while no overlapping between standard deviation values of fruit crops and bare soil, therefore, the supervised classification was performed for each of fruit crops and bare soil, and finally the remaining area of the region was assigned to other crops. The accuracy of the classification methodology was assessed by:

1-Calculating the percent deviation of supervised classified surface area of fruit crops and other corps from the official statistics of crop surface area obtained from Ministry of Agriculture Murakaba office in Tiba region (Personal Communication).

2-Overlaying the ground-truth points for each group of data over the classified images.

- **Geo-spatial distribution of analyzed and predicted bare soil data:**

Significant predicted bare soil data obtained from multiple linear regression analysis (CC and EC) were GIS-interpolated as a raster surface from data points by using the inverse distance weighed (IDW) technique and were compared with same interpolated raster maps of laboratory analyzed data points. Interpolated maps were supervised classified by ArcGIS procedures to 3 categories: CC (0.0 – 4.0, 4.1 – 8.0, and > 8 %); EC (0.0 – 2.0, 2.1 – 4.0, and > 4 $dS \cdot m^{-1}$); and SMU (A, B, and C). GIS maps of soil

mapping units (SMU) were generated by summing values for each raster layer on a cell-by-cell basis in each group of layers (analyzed & predicted). As for SMU basis for classification (Richards, 1954 and Black *et al*., 1965), the following was considered:

1-CC values: 2.0 – 4.0 % (non-calcareous), 4.1 – 8.0 % (slightly-calcareous), and > 8 % (moderately-calcareous).

2-EC values: 1.4 - 2.0 $dS \cdot m^{-1}$ (non-saline), 2.1 – 4.0 $dS \cdot m^{-1}$ (slightly saline), and > 4 $dS \cdot m^{-1}$ (moderately saline).

The accuracy of bare soil characterization prediction model was assessed by calculating the areas in each category for both analyzed and predicted data and calculate the percent deviation.

RESULTS AND DISCUSSION

1)Spectral signature analysis:

Location of Tiba region in western Nile delta and the composite image of Tiba region extracted from Landsat-8 OLI satellite imagery are presented in Figures (1&2). The total surface area of Tiba region was calculated by ArcGIS and was found to be 38266.45 Faddan. Figure 3, illustrates the GPS locations of ground-truth points for all crop types and bare soil sites collected during the investigation. The total number of sites visited and GPS collected were 2040, composed of 1694 site for fruit crops, 292 site for other crops, and 54 site for bare soil. GPS collection for each type was done randomly in selected areas clustered at upper and middle parts of Tiba region based on general field variability in soil and crop productivity form field experience in the area. The number of location varied from 679 sites for oranges and 384 for grapes, to 4 sites in plum and 3 sites for tomatoes, and this variability indicates the actual density of each crop type as orange and grape representing the most common cropping patter in Tiba whereas plum and tomato were the lowest. The spectral signature curve of band reflectance for each crop type and bare soil are illustrated in Figure (4-A). The spectral reflectance curve of bare soil was higher in the visible region of the spectrum from band 1 (0.43-0.45 µm) to band 4 (0.64-0.67 µm), declined a little in band 5 of near infrared (NIR; 0.85-0.88 µm), then continued to be the highest in band 6 and 7 of short wave infrared 1 & 2 (SWIR1 & SWIR2; 1.57-2.29 µm). Crop spectral signature curves followed the same pattern of bare soil but were lower in value than the soil curve, except at band 5 where sugarbeet was the highest. In general, field and vegetable crops were the lowest in reflectance values and fruit crops were in-between, with wheat values representing the lowest reflectance values in all bands except band 5 where several interaction occurred. Previous research reported that soil spectral signature curve has higher reflectance in the visible spectrum (Blue, Green, and RED) than healthy green vegetation and lower reflectance than unhealthy or dead vegetation, whereas in the NIR, soil has lower reflectance than both healthy and dead vegetation. Also, dead or dormant vegetation had higher reflectance curve than healthy vegetation in the visible spectrum but

lower in the NIR (Perry and Lautenschlager, 1984). As Figure (4A) shows, there was a close interaction in several points for each band and a Post-Hoc Tukey test was run for crop reflectance values for each band (data not presented) and no significant differences were found among bare soil, fruit crops, vegetable crops and field crops (p-value < 0.05), and this result was due to the high standard deviation values (SD) from the mean among individual crops. A defining characteristic of small-scale farming in Tiba region as well as in many regions in Egypt is the spatial fragmentation, crop diversity due to over cropping, and within field variability related to the farmer background and experience. I concluded that, it is impossible to separate and run a supervised classification among individual crops based on individual band reflectance values. Therefore, I pooled together the data of reflectance values of fruit corps (orange, mandarin, lime & lemon, grape, apple, peach, apricot, plum, guava, mango, and cactus pear), other crops (tomato, squash, wheat, berseem clover, broad bean, and sugarbeet), while bare soil values remained as it is (Figure 4B), to test whether it is possible to have a significant differences among them. Data presented in Figure (4B) and Table (1), show that there were significant differences (p-value < 0.05) among fruit crops, other crops, and bare soil in all reflectance values of band 1, 2, 3, 4, 6, 7 & 8, whereas no significant difference was found in band 5 between other crops and bare soil but both were significantly different from fruit corps. Bare soil reflectance values were the highest in all bands and ranging from 0.193 (band 1) to 0.442 (band 6), followed by fruit crops with reflectance value from 0.161 (band 1) to 0.361 (band 5), and the lowest reflectance values were for the other crops and ranged from 0.150 (band 1) to 0.409 (band 5).

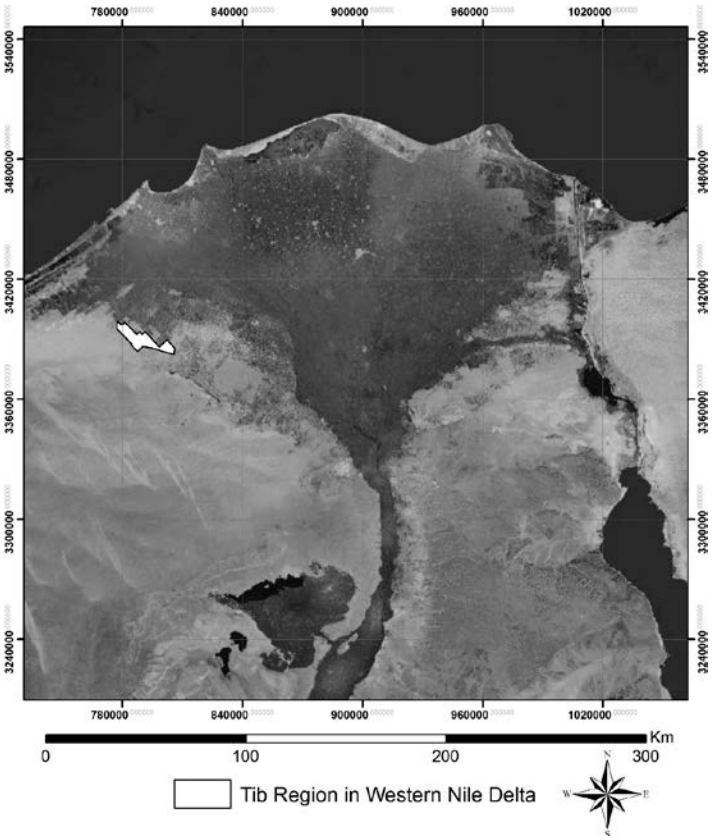

Figure (1): Location of Tiba region in western Nile delta of Egypt.

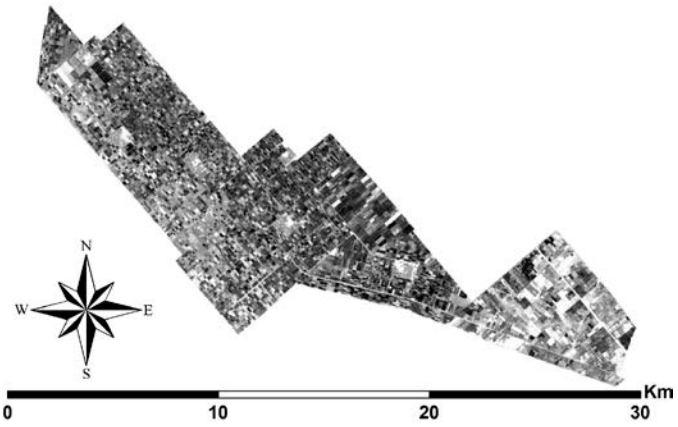

Figure (2): Landsate-8 satellite composite image of Tiba region.

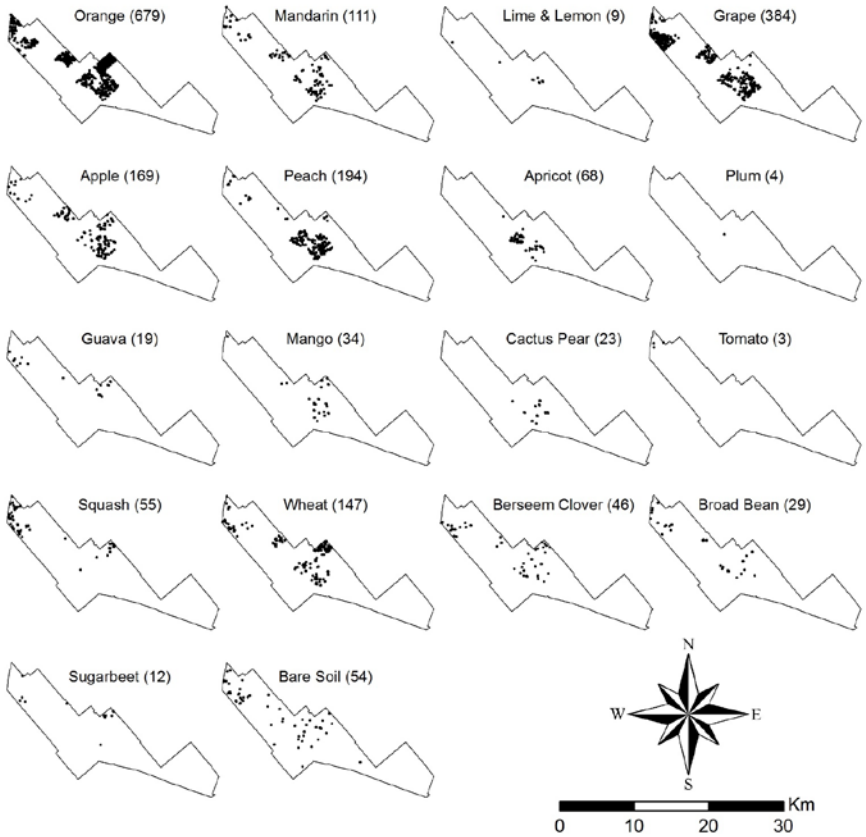

Figure (3): Global positioning system (GPS) locations and number of ground-truth sites for each crop type and bare soil.

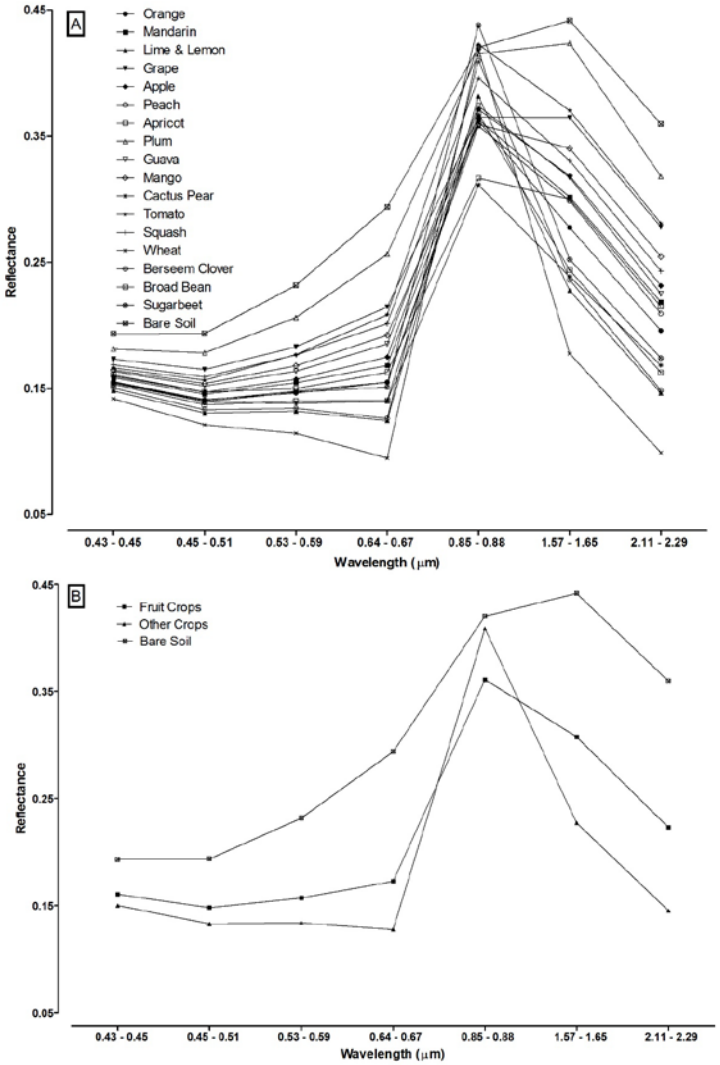

Figure (4): Individual spectral signature curves (A), and grouped spectral signature curves (B) for crops and bare soil.

2)Vegetation indices analysis:

Table (1) presents the vegetation indices (VIs) values for each group, and there were significant differences among all groups for all the 9 VIs. Value of Normalized Difference Vegetation Index (NDVI) was highest for other crops (0.531), followed by fruit crops (0.362), and the lowest was bare soil (0.180). As for Ratio Vegetation Index (RVI), bare soil value recorded the highest (0.697), fruit crops value was in the middle (0.477), and the lowest was the other crops (0.324). Transformed Vegetation Index (TVI) pattern was similar to NDVI, with mean values of 1.012, 0.927, and 0.824, for other crops, fruit crops, and bare soil, respectively. Value distribution for Ashburn Vegetation Index (AVI), Soil-Adjusted Vegetation Index (SAVI), and Modified Soil-Adjusted Vegetation Index 2 (MSAVI2) were similar and peaked in other crops, followed by fruit crops, and were lowest for bare soil. Regarding the Tasseled Cap VIs, the pattern of values for Tasseled Cap Brightness (TCB) was similar to RVI, as bare soil was the highest (0.789), followed by fruit crops (0.570), and other crops the lowest (0.509). Tasseled Cap Greenness (TCG) and Tasseled Cap Wetness (TCW) were similar in the general pattern of values, with TCW has a negative values and was highest in other crops (-0.0002), followed by fruit crops (-0.087), and the lowest was for bare soil (-0.164).). VIs are single numbers derived from mathematical models for the spectral reflectance of two or more wavelength bands of the electromagnetic spectrum (Ji and Peters, 2007). VIs models are primarily designed to optimized vegetation signals, decouple the canopy background noise, and reduce the atmospheric effects (Pettorell *et al*., 2005).

Table (1): Band reflectance and vegetation indices values derived from Landsat-8 OLI remote sensing data for fruit crops, other crops, and bare soil in Tiba region.

	Fruit Crops	Other Crops	Bare Soil
	Band reflectance (mean ± SD)		
Band 1	0.161±0.012 b*	0.150±0.015 c	0.193±0.014 a
Band 2	0.148±0.017 b	0.133±0.020 c	0.194±0.019 a
Band 3	0.157±0.028 b	0.134±0.033 c	0.232±0.029 a
Band 4	0.173±0.047 b	0.128±0.057 c	0.294±0.045 a
Band 5	0.361±0.033 b	0.409±0.053 a	0.420±0.039 a
Band 6	0.308±0.069 b	0.227±0.088 c	0.442±0.059 a
Band 7	0.223±0.067 b	0.145±0.082 c	0.360±0.057 a
Band 8	0.160±0.035 b	0.126±0.043 c	0.258±0.035 a
	Vegetation index (mean ± SD)		
NDVI	0.362±0.107 b	0.531±0.168 a	0.180±0.046 c
RVI	0.477±0.116 b	0.324±0.161 c	0.697±0.065 a
TVI	0.927±0.057 b	1.012±0.086 a	0.824±0.028 c
AVI	0.189±0.045 b	0.281±0.086 a	0.127±0.024 c
SAVI	0.276±0.073 b	0.408±0.127 a	0.157±0.035 c
MSAVI2	0.261±0.072 b	0.403±0.135 a	0.151±0.033 c
TCB	0.570±0.090 b	0.509±0.100 c	0.789±0.090 a
TCG	0.074±0.040 b	0.149±0.071 a	0.007±0.023 c
TCW	-0.087±0.055 b	-0.0002±0.077 a	-0.164±0.045 c

*** Mean ± SD; separation within rows by the Post-Hoc Tukey Test at P-value < 0.05 (lowercase letters).**

3)Supervised classification analysis:

Figure (5) illustrates the raster maps of supervised classification of Landsat-8 OLI band reflectance for cropping pattern of fruit crops, other crops and bare soil areas in Tiba region, and the estimated surface area from satellite remote sensing for cropping pattern for each classified band and percent deviation of estimated data from the data obtained from Ministry of agriculture (MOA) were presented (Table 2).

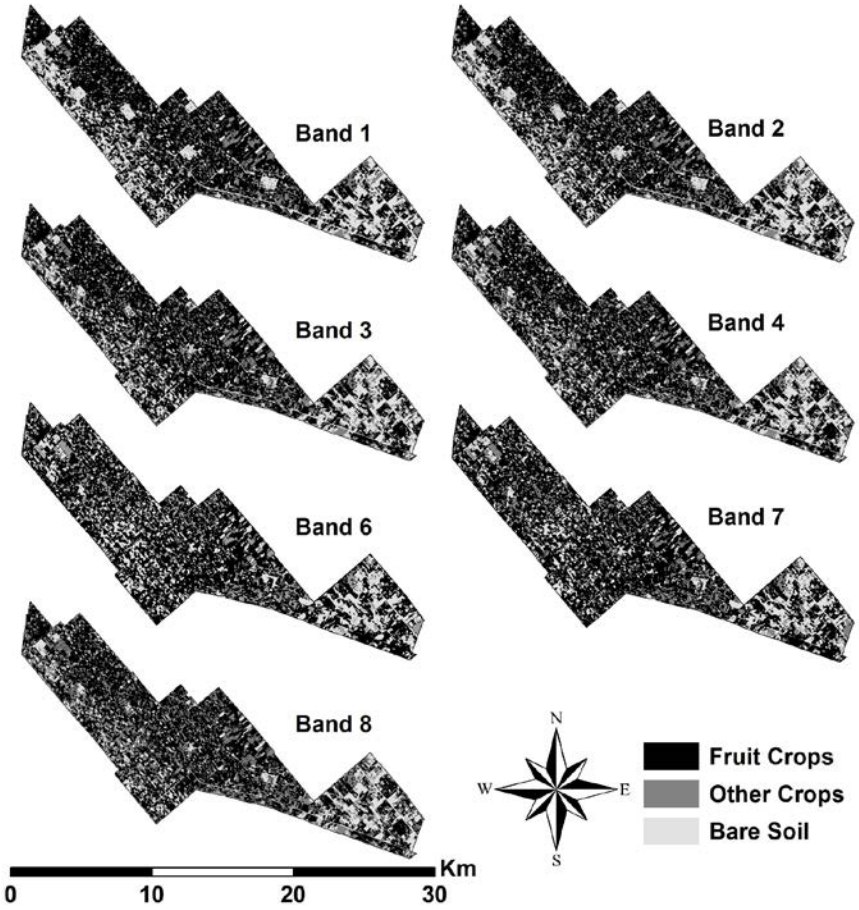

Figure (5): Supervised classification of Landsat-8 OLI band reflectance for cropping pattern of fruit crops, other crops and bare soil areas in Tiba region.

Table (2): Estimated surface area of supervised classified band reflectance of Landsat-8 OLI for fruit crops, other crops and bare soil areas in Tiba region.

	Band 1			Band 2			Band 3			Band 4		
	Classified area		*Dev.	Classified area		Dev.	Classified area		Dev.	Classified area		Dev.
	Faddan	%	%	Faddan	%	%	Faddan	%	%	Faddan	%	%
Fruit Crops	21375.42	55.86	-2.39	20875.74	54.55	-4.67	21761.74	56.87	-0.63	21710.58	56.74	-0.86
Other Crops	8995.38	23.51	-24.46	10046.14	26.25	-15.64	10320.99	26.97	-13.33	10759.99	28.12	-9.64
Bare Soil	7895.65	20.63	---	7344.56	19.19	---	6183.72	16.16	---	5795.88	15.15	---
Total	38266.45	100	---	38266.45	100	---	38266.45	100	---	38266.45	100	---

	Band 6			Band 7			Band 8		
	Classified area		Dev.	Classified area		Dev.	Classified area		Dev.
	Faddan	%	%	Faddan	%	%	Faddan	%	%
Fruit Crops	23362.50	61.05	6.68	22983.30	60.06	4.95	21001.06	54.88	-4.10
Other Crops	7052.84	18.43	-40.77	8148.11	21.29	-31.57	11631.96	30.40	-2.32
Bare Soil	7851.11	20.52	---	7135.04	18.65	---	5633.42	14.72	---
Total	38266.45	100	---	38266.45	100	---	38266.45	100	---

***% Deviation = ((classified – MOA statistics[1])/MOA statistics) × 100**

[1]MOA statistics = ministry of agriculture statistics in Tiba region (Murakaba Office) for fruit and other crops, 21899 and 11908 Faddan, respectively.

4)Integration approach with statistical analysis:

A) Cropping pattern and bare soil areas:

As for fruit crops surface area estimations, the least deviated and most accurate values were obtained from band 3 (21761.74 Faddan; 56.87 % of total surface area; -0.63 % deviation) and band 4 (21710.58 Faddan; 56.74 % of total surface area; -0.86 % deviation), the middle deviated value was for band 1 (-2.39 % deviation), whereas the highest deviated values were for band 8, 2, 7, and 6 (-4.10, -4.67, 4.95, and 6.68 % deviation, respectively). As regard to other crops surface area estimations, band 8 had the minimum deviated value from MOA data (11631.96 Faddan; 30.40 % of total area; -2.32 % deviation), band 4, 3, and 2 had a middle deviated values (-9.64, -13.33, and -15.64 % deviation, respectively), while band 1, 7, and 6 had the maximum deviated values (-24.46, -31.57, and -40.77 % deviation, respectively). Figure (6) & Table (3) illustrated the results of estimated surface area of cropping pattern by using the VIs. calculated from Landsat-8 OLI reflectance data. The closest estimated values of fruit crops to MOA data were for AVI and TCB (-6.46 and 6.82 % deviation), middle values for MSAVI2, SAVI, and TCG (-7.81, -8.81, and -8.99 % deviation, respectively), and the distant values were for NDVI, TVI, RVI, and TCW (-9.32, -9.66, -9.84, and 11.62 % deviation, respectively). As for other crops estimation, the least deviated values for estimates were for RVI, NDVI, TVI, and TCB (-22.94, -24.85, -23.73, and -25.25 % deviation, respectively), whereas the highest deviated values were for SAVI, TCG, AVI, MSAVI2, and TCW (-37.03, -38.41, -41.23, -42.00, and -45.19 % deviation, respectively). The results of the first assessment method of MOA statistics indicated that band reflectance estimates for cropping pattern were more precise and least deviated from those estimates by using VIs for both fruit crops and vegetable crops. Few studies have evaluated the characteristics of Landsat-8 OLI derived vegetation indices compared with previous available research with other satellite sensors (Ke *et al*., 2015). The reduced accuracy of VIs can be explained from the overlapping of spectral signature curves at NIR band 5

(0.85-0.88 µm) for bare soil and some crops (Figure 4A), as well as due to the failure of Post-Hoc test to distinguish significantly between fruit crops and both other crops and bare soil (Table 1), as all VIs calculation equations require the value of NIR. Chlorophyll pigments in healthy plant leaves absorb Blue and RED wavelength of the visible spectrum to perform photosynthesis, whereas mesophyll cells scatters the NIR region of the electromagnetic spectrum, and therefore all VIs equations use both RED and NIR to separate the green vegetation biomass from the surrounding environment (Pettorell *et al*., 2005). Therefore, under the conditions of our study, it is recommend to use reflectance data of Landsat-8 OLI band 3 or 4 to estimate surface area of fruit crops. As regard to the second accuracy assessment method for the previous discussed estimates of fruit crops area, the results of overlaying all ground-truth points with the classified band 3 & 4 were deviated by values of -24.9 and -25.6%, respectively. Comparing these data with the first assessment methodology of MOA statistics for fruit crops and other crops with total deviated values of -14.0 and -10.5% for band 3 & 4, respectively, the differences between the two assessment methods maybe partially attributed on the one hand to variability in soil mapping units, soil productivity, farmer's practices and experiences, crop physiological status related to irrigation, fertilization, pruning, and health management, as well as, planting density, vine training and tree high, crop variability in age, cultivated variety, rootstock, and microclimate variations in different locations around crops. On the other hand, difference may also be partially attributed to inaccuracy of MOA statistics, as it's often difficult to collect accurate cropping pattern in short time by field visits for each growing season and every year. While data estimates for area of fruit crop was positively correlated with the official MOA census, there was still deviation between agricultural data and remote sensing derived data; similar results was previously reported during assessment of citrus groves by remote sensing in Florida, USA (Shrivastava and Gebelein, 2007).

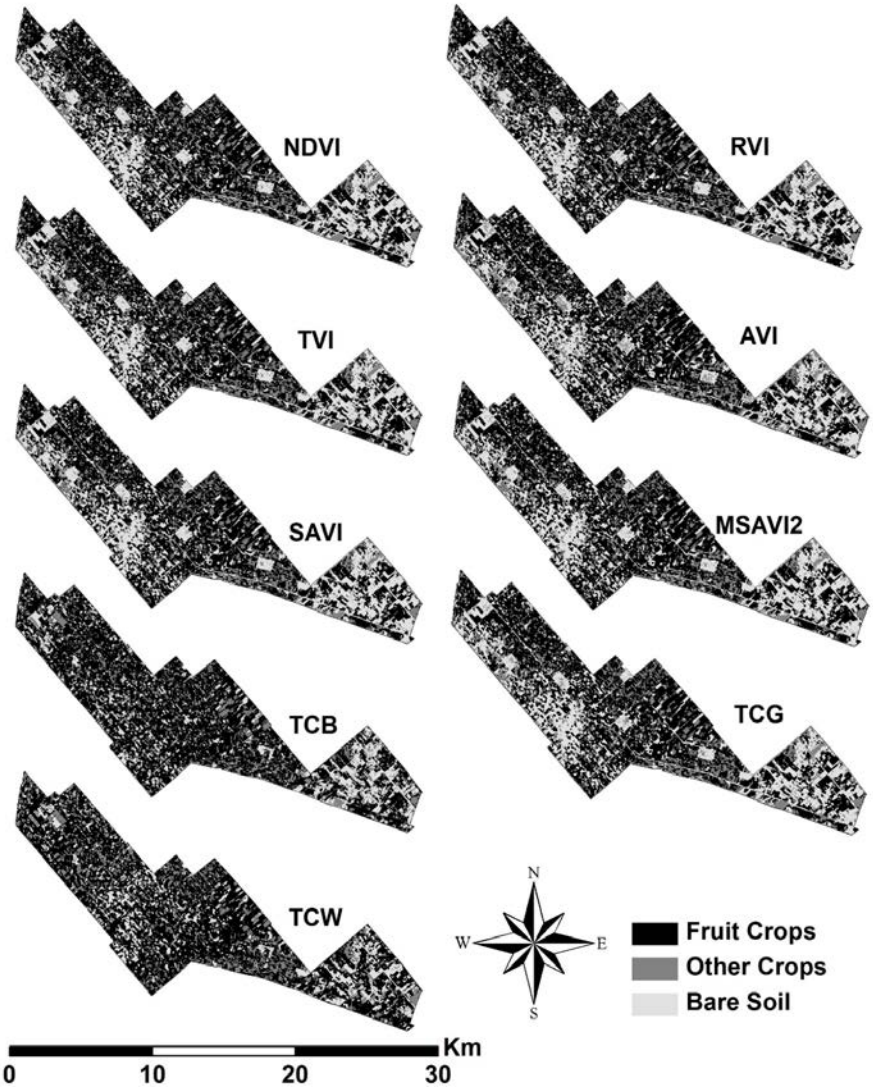

Figure (6): Supervised classification of Landsat-8 OLI calculated vegetation indices (VIs) for cropping pattern of fruit crops, other crops and bare soil areas in Tiba region.

Table (3): Estimated surface area of supervised classified vegetation indices (VIs) derived from Landsat-8 OLI remote sensing data for fruit crops, other crops and bare soil in Tiba region.

	NDVI			RVI			TVI		
	Classified area		*Dev. %	Classified area		Dev. %	Classified area		Dev. %
	Faddan	%		Faddan	%		Faddan	%	
Fruit Crops	19858.64	51.90	-9.32	19743.38	51.59	-9.84	19784.44	51.70	-9.66
Other Crops	8948.64	23.39	-24.85	9175.77	23.98	-22.94	9081.88	23.73	-23.73
Bare Soil	9459.16	24.72	---	9347.29	24.43	---	9400.12	24.56	---
Total	38266.45	100	---	38266.45	100	---	38266.45	100	---
	AVI			SAVI			MSAVI2		
	Classified area		Dev. %	Classified area		Dev. %	Classified area		Dev. %
	Faddan	%		Faddan	%		Faddan	%	
Fruit Crops	20483.48	53.53	-6.46	19970.00	52.19	-8.81	20187.80	52.76	-7.81
Other Crops	6997.84	18.29	-41.23	7497.96	19.59	-37.03	6906.69	18.05	-42.00
Bare Soil	10785.13	28.18	---	10798.48	28.22	---	11171.96	29.20	---
Total	38266.45	100	---	38266.45	100	---	38266.45	100	---
	TCB			TCG			TCW		
	Classified area		Dev. %	Classified area		Dev. %	Classified area		Dev. %
	Faddan	%		Faddan	%		Faddan	%	
Fruit Crops	23392.85	61.13	6.82	19929.37	52.08	-8.99	24444.76	63.88	11.62
Other Crops	8900.98	23.26	-25.25	7333.83	19.17	-38.41	6526.61	17.06	-45.19
Bare Soil	5972.61	15.61	---	11003.25	28.75	---	7295.08	19.06	---
Total	38266.45	100	---	38266.45	100	---	38266.45	100	---

***% Deviation = ((classified – MOA statistics[1])/MOA statistics) × 100**

[1]MOA statistics = ministry of agriculture statistics in Tiba region (Murakaba Office) for fruit and other crops, 21899 and 11908 Faddan, respectively.

B) Soil mapping units (SMU):

Table (4) presents the multiple linear regression modeling (MLRM) equations to predict bare soil calcium carbonate (CC) %, electrical conductivity (EC) in $dS \cdot m^{-1}$, pH, and soil texture (sand, silt, and clay %) by using Landsat-8 OLI band reflectance (band 1 to band 8) data of bare soil as regressors. MLRM was highly significant for CC and EC (p-value <0.01) and the effect size (R^2) values were 0.868 and 0.803 for CC and EC, respectively, indicating very high prediction accuracy. MLRM was not significant for pH and soil texture, and the R^2 values were 0.574, 0.476, 0.515, and 0.391 for pH, sand, silt and clay, respectively. The coefficient of variation (C.V.) was calculated for analyzed and predicted data and was high for CC (44.5 & 41.4, for analyzed & predicted, respectively) and EC (53.9 & 48.3, for analyzed & predicted, respectively), but was very low for pH and soil texture, and these values confirm the significance of MLRM prediction for CC and E.C as variables with high variations capable of distinguishing among different soil units. Therefore, only CC and EC data were chosen as characteristics for bare soil classification to SMU. As for the range of soil data before classification, the minimum values for analyzed and predicted CC were 2.02 & 2.04%, and the highest were 10.16 & 9.65%, respectively, whereas for EC, the minimum were 1.40 & 1.44 $dS \cdot m^{-1}$, and the maximum 8.66 & 7.61 $dS \cdot m^{-1}$, for analyzed & predicted, respectively. Figure (7) illustrates the geo-spatial interpolation maps of analyzed and predicted data for CC, EC and the derived SMU in Tiba region for both. The calculated area of classified categories of CC, EC and SMU with percent deviation of predicted from analyzed, were presented in Table (5). As for CC data, 82.22% of total area

predicted was in the second category ranging from 4.1 to 8.0 % CC and were least deviated (3.02%), followed by 15.67 % of total area located in first category ranging from 0 to 4 % CC and deviated by -9.94%, and the remaining 2.11 % of Tiba was located in the third category of > 8 % CC and was -24.30% deviated from analyzed data (Table 5). Regarding EC predicted data, 72.63% of classified area located in second category of EC ranging 2.1-4.0 $dS \cdot m^{-1}$ and deviated by 2.51%, 26.41% of Tiba area was in third category of EC > 4 $dS \cdot m^{-1}$ and -6.53 % deviated, and the remaining 0.97% of area was allocated for the first category of EC ranging 0-2 $dS \cdot m^{-1}$ and deviated by 7.52 % from analyzed data. Concerning SMU, 58.11% of total Tiba area was allocated to unit B (slightly-calcareous & non- to slightly-saline) and deviated by 6.92% from analyzed, 26.22 % of area allocated to unit C (slightly- to moderately-calcareous & moderately-saline) and deviated by -7.19 %, and the other 15.67% area was allocated to unit A (non-calcareous & non- to slightly-saline) and deviated by -9.94 % (Table 5). This research showed the credibility of using satellite remote sensing data of Landsat-8 OLI to predict main surface bare soil characteristics in Tiba region as in most Tiba area CC, EC, and SMU were predicted with high accuracy and least deviation from analyzed data. Ismail *et al*., (2012), reported on a study for potential of irrigated agriculture in the western side of the Nile Delta that the most soil limiting factors were soil depth, drainage, slope gradient, salinity, and available water holding capacity. Spatial heterogeneity of surface bare soil is an important inherent property that describes the natural variability of the region and Landsat-8 modern sensors can detect the differences and describe the landscape (Ding *et al*., 2014). Conventional soil analyses are too expensive to capture soil heterogeneity at regional scale with the needed geo-spatial resolution, and remote sensing prediction technique can deliver precise details at low cost (Patzold *et al*., 2008).

Table (4): Multiple linear regression modeling to predict bare soil calcium carbonate (CC), electrical conductivity (EC), and soil texture by using band reflectance of bare soil as regressors.

	Regression parameters [1]	
	Model	**R^2**
CC(%)	$- 37.969 + 574.255 X_1 - 130.107 X_2 - 218.253 X_3 + 127.505 X_4 + 5.812 X_5 + 44.022 X_6 - 35.478 X_7 - 148.417 X_8$	0.868*
EC($dS \cdot m^{-1}$)	$20.791 - 1086.010 X_1 + 1390.953 X_2 - 410.512 X_3 + 78.343 X_4 + 59.859 X_5 - 0.278 X_6 + 14.003 X_7 - 129.895 X_8$	0.803*
pH	$8.244 + 39.621 X_1 - 54.592 X_2 + 6.981 X_3 + 21.403 X_4 - 0.505 X_5 - 0.098 X_6 - 0.837 X_7 - 19.356 X_8$	0.574
Sand (%)	$104.594 - 172.236 X_1 + 120.019 X_2 + 9.645 X_3 - 27.380 X_4 - 3.510 X_5 + 24.189 X_6 - 17.447 X_7 + 26.675 X_8$	0.476
Silt (%)	$- 0.469 + 51.619 X_1 - 37.285 X_2 + 1.658 X_3 + 15.320 X_4 + 1.124 X_5 - 9.007 X_6 + 6.522 X_7 - 20.401 X_8$	0.515
Clay (%)	$- 4.124 + 120.617 X_1 - 82.734 X_2 - 11.303 X_3 + 12.060 X_4 + 2.387 X_5 - 15.182 X_6 + 10.925 X_7 - 6.275 X_8$	0.391

[1] Regression enter method, X_1=Band 1, X_2=Band 2, X_3=Band 3, X_4=Band 4, X_5=Band 5, X_6=Band 6, X_7=Band 7, X_8=Band 8, R^2= effect size, * significant at P-value <0.01.

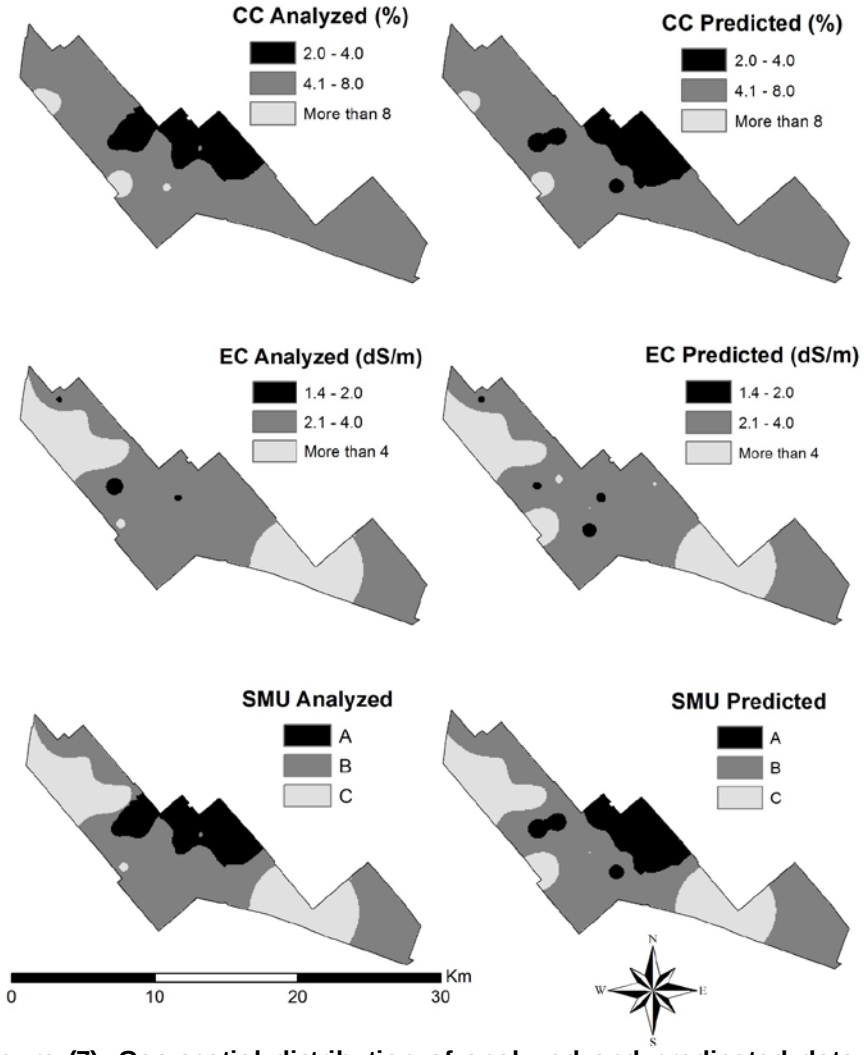

Figure (7): Geo-spatial distribution of analyzed and predicated data of Landsat-8 OLI satellite for soil calcium carbonate (CC) and electrical conductivity (EC), and derived soil mapping units (SMU) in Tiba region. SMU (A): non-calcareous & non- to slightly-saline, (B): slightly-calcareous & non- to slightly-

saline, (C): slightly- to moderately-calcareous & moderately-saline.

Table (5): Predicated compared with analyzed values and accuracy assessment derived for evaluating performance of Landsat-8 OLI satellite remote sensing prediction model to estimate soil calcium carbonate (CC), electrical conductivity (EC), and soil mapping units (SMU) in Tiba region.

CC					
Range in Soil (%)	**Analyzed**		**Predicted**		
	Classified area		**Classified area**		***Dev.**
	Faddan	%	Faddan	%	%
0.0– 4.0	6659.93	17.40	5997.69	15.67	-9.94
4.1 – 8.0	30542.02	79.81	31462.95	82.22	3.02
> 8.0	1064.50	2.78	805.81	2.11	-24.30
Total	38266.45	100	38266.45	100	---
EC					
Range in Soil ($dS \cdot m^{-1}$)	**Analyzed**		**Predicted**		
	Classified area		**Classified area**		**Dev.**
	Faddan	%	Faddan	%	%
0.0– 2.0	344.06	0.90	369.92	0.97	7.52
2.1 – 4.0	27111.81	70.85	27792.16	72.63	2.51
> 4.0	10810.58	28.25	10104.36	26.41	-6.53
Total	38266.45	100	38266.45	100	---
SMU					
Unit	**Analyzed**		**Predicted**		
	Classified area		**Classified area**		**Dev.**
	Faddan	**%**	**Faddan**	**%**	**%**
A	6659.93	17.40	5997.69	15.67	-9.94
B	20795.94	54.35	22235.54	58.11	6.92
C	10810.58	28.25	10033.22	26.22	-7.19
Total	38266.45	100	38266.45	100	---

***% Deviation = ((Predicted – Analyzed)/Analyzed)) ×10**

CONCLUSION

I concluded that the accuracy of cropping pattern classification achieved in this research was attributed mainly to success in identifying the spectral signature of fruit crops and bare soil which enabled the classification procedures by using individual band reflectance and VIs derived from Landsat-8 remote sensing data. Further research is needed to investigate the use of multiple band classification approach which may enhance and enable the separation of particular crop type. Temporal classification studies at different crop phonological stages during the season may reveal further interesting details, accuracy, and approaches. Validation assessment for cropping pattern classification in western Nile delta by applying the technique developed in this study to other areas than Tiba will evaluate the robustness of the technique and the potentially for use over larger reclaimed areas in Egypt.

ACKNOWLEDGMENT

The author would like to thank Project: Collective action and agricultural productivity in Egypt's new lands (Nasr canal area); Science & Technology Development Fund, STDF-IRD Joint Innovation Projects, Fund No. 4652, for funding field activities of this research. (Project Egyptian PI: Dr. Diaa O. El-Ansary, Precision Agricultural Laboratory, Department of Pomology, Faculty of Agriculture, El-Shatby, University of Alexandria, Alexandria, Egypt).

REFERENCES

Baig, M. H. A., L. Zhang, T. Shuai, and Q. Tong (2014). Derivation of a tasselled cap transformation based on Landsat 8 at-satellite reflectance. Remote Sensing Letters, 5 (5): 423 – 431.

Black, C. A., D. D. Evans, J. L. White, L. E. Ensminger, and F. E. Clark (1965). Methods of Soil Analysis. Part 1. Physical and Mineralogical Properties, Including of Statistics of Measurement and Sampling. American Society of Agronomy, Inc., Madison Publisher, Wisconsin, USA.

Chander, G., B. L. Markham, and D. L Helder (2009). Summary of current radiometric calibration coefficients for Landsat MSS, TM, ETM+, and EO-1 ALI sensors. Remote Sensing of Environment, 113: 893 – 903.

Ding, Y., K. Zhao, X. Zheng, and Tao Jiang (2014). Temporal dynamics of spatial heterogeneity over cropland quantified by time-series NDVI, near infrared and red reflectance of Landsat 8OLI imagery. International Journal of Applied Earth Observation and Geoinformation, 30: 139 – 145.

González-Dugo, M. P., S. Escuin, F. Cano, V. Cifuentes, F. L. M. Padilla, J. L. Tirado, N. Oyonarte. P. Fernández, and L. Mateos (2013). Monitoring evapotranspiration of irrigated crops using crop coefficients derived from time series of satellite images. II. Application on basin scale. Agricultural Water Management, 125: 92 – 104.

Heiniger, R. W. (1999). Understanding geographic information systems and global positioning systems in horticultural applications. HortTech., 9: 539-547.

Ismail, M., M. K. Abdel Ghaffar, and M. A. Azzam (2012). GIS application to identify the potential for certain irrigated agriculture uses on some soils in Western Desert, Egypt. The Egyptian Journal of Remote Sensing and Space Sciences, 15: 39 – 51.

Ji, L. and A. J. Peters (2007). Performance evaluation of spectral vegetation indices using a statistical sensitivity function. Remote Sensing of Environment, 106: 59 – 65.

Jiang, Z., A. R. Huete, J. Li, and Y. Chen (2006). An analysis of angle-based with ratio-based vegetation indices. IEEE Transactions on Geoscience and Remote Sensing, 44 (9): 2506 – 2513.

Ke, Y., J. Im, J. Lee, H. Gong, and Y. Ryu (2015). Characteristics of Landsat 8 OLI-derived NDVI by comparison with multiple satellite sensors and *in-situ* observations. Remote Sensing of Environment, 164: 298 – 313.

Kolios, S. and C. D. Stylios (2013). Identification of land cover/land use changes in the greater area of the Preveza peninsula in Greece using Landsat satellite data. Applied Geography, 40: 150 – 160.

Laosuwan, T. and P. Uttaruk (2014). Estimating tree biomass via remote sensing, MSAVI 2, and Fractional Cover Model. IETE Technical Review, 31 (5): 362 – 368.

Lopez-Granados, F., M. T. Gomez-Casero, J. M. Pena-Barragan, M. Jurado-Exposito, and L. Garcıa-Torres (2010). Classifying irrigated crops as affected by phenological stage using discriminant analysis and neural networks. J. Amer. Soc. Hort. Sci., 135 (5): 465 – 473.

Maeda, E. E., J. Heiskanen, K. W. Thijs, and P. K. E. Pellikka (2014). Season-dependence of remote sensing indicators of tree species diversity. Remote Sensing Letters, 5 (5): 404 – 412.

Maselli, F., M. Chiesi, L. Brilli, and M. Moriondo (2012). Simulation of olive fruit yield in Tuscany through the integration of remote sensing and ground data. Ecological Modelling, 244: 1 – 12.

Mateos, L., M. P. González-Dugo, L. Testi, and F. J. Villalobos (2013). Monitoring evapotranspiration of irrigated crops using crop coefficients derived from time series of satellite images. I. Method validation. Agricultural Water Management, 125: 81 – 91.

Othman, Y., C. Steele, D. VanLeeuwen, R. Heerema, S. Bawazir, and R. St. Hilaire (2014). Remote sensing used to detect moisture status of pecan orchards grown in a desert environment. International Journal of Remote Sensing, 35 (3): 949 – 966.

Papes, M., R. Tupayachi, P. Martinez, A. T. Peterson, G. P. Asner, and G. V. N. Powell (2013). Seasonal variation in spectral signatures of five genera of rainforest trees. IEEE Journal of Selected Tropics in Applied Earth Observations and Remote Sensing, 6 (2): 339 – 350.

Patzold, S., F. M. Mertens, L. Bornemann, B. Koleczek, J. Franke, H. Feilhauer, and G. Welp (2008). Soil heterogeneity at the field scale: a challenge for precision crop protection. Precision Agric., 9: 367 – 390.

Paudel, D., J. K. Thakur, S. K. Singh, and P. K. Srivastava (2015). Soil characterization based on land cover heterogeneity over a tropical landscape: an integrated approach using earth observation data-sets. Geocarto International, 30 (2): 218 – 241.

Perry, C. R., Jr. and L. F. Lautenschlager (1984). Functional equivalence of spectral vegetation indices. Remote Sensing of Environment, 14: 169 – 182.

Pettorell, N., J. O. Vik, A. Mysterud, J. Gaillard, C. J. Tucker, and N. C. Stenseth (2005). Using the satellite-derived NDVI to assess ecological responses to environmental change. Trends in Ecology and Evolution, 20 (9): 503 – 510.

Qin, Y., X. Xiao, J. Dong, Y. Zhou, Z. Zhu, G. Zhang, G. Du, C. Jin, W. Kou, J. Wang, and X. Li (2015). Mapping paddy rice planting area in cold temperate climate region through analysis of time series Landsat 8 (OLI), Landsat 7 (ETM+) and MODIS imagery. ISPRS Journal of Photogrammetry and Remote Sensing, 105: 220–233.

Reis, S. and K. Tasdemir (2011). Identification of hazelnut fields using spectral and Gabor textural features. ISPRS Journal of Photogrammetry and Remote Sensing, 66: 652 – 661.

Reynolds, A. and J. H. Rezaei (2014). Spatial variability in Ontario Cabernet Franc vineyards: I. Interrelationships among soil composition, soil texture, soil and vine water status. Journal of Applied Horticulture, 16 (1): 3 - 23.

Rhew, I. C., A. V. Stoep, A. Kearney, N. L. Smith, and M. D. Dunbar (2011). Validation of the normalized difference vegetation index as a measure of neighborhood greenness. AEP, 21(12): 946 – 952.

Richards, R. L., (ed.) (1954). Diagnosis and Improvement of Saline and Alkali Soils. Agriculture Handbook No. 60, U.S. Gov. Printing Office, Washington, USA.

Richardson, A. J. and C. L. Wiegand (1977). Distinguishing vegetation from soil background information. Photogrammetric Engineering and Remote Sensing, 43(12): 1541 – 1552.

Roy, D. P., M. A. Wulder, T. R. Loveland, C. E. Woodcock, R. G. Allen, M. C. Anderson, D. Helder, J. R. Irons, D. M. Johnson, R. Kennedy, T. A. Scambos, C. B. Schaaf, J. R. Schott, Y. Sheng, E. F. Vermote, A. S. Belward, R. Bindschadler, W. B. Cohen, F. Gao, J. D. Hipple, P. Hostert, J. Huntington, C. O. Justice, A. Kilic, V. Kovalskyy, Z. P. Lee, L. Lymburner, J. G. Masek, J. McCorkel, Y. Shuai, R. Trezza, J. Vogelmann, R .H. Wynne, and Z. Zhu (2014). Landsat-8: Science and product vision for terrestrial global change research. Remote Sensing of Environment, 145: 154 – 172.

Serra, P. and X. Pons (2013). Two Mediterranean irrigation communities in front of water scarcity: A comparison using satellite image time series. Journal of Arid Environments, 98: 41 – 51.

Shrivastava, R. J. and J. L. Gebelein (2007). Land cover classification and economic assessment of citrus groves using remote sensing. ISPRS Journal of Photogrammetry & Remote Sensing, 61: 341 –353.

Tapia-Silva, F., S. Itzerott. S. Foerster, B. Kuhlmann, and H. Kreibich (2011). Estimation of flood losses to agricultural crops using remote sensing. Physics and Chemistry of the Earth, 36: 253 – 265.

Tucker, C. J. (1979). Red and photographic infrared linear combinations for monitoring vegetation. Remote Sensing of Environment, 8: 127 – 150.

التعرف على البصمة الطيفية وتقدير مساحة السطح المنزرعة بمحاصيل الفاكهة في منطقة طيبة الواقعة في غرب دلتا النيل في مصر بإستخدام بيانات الإستشعار عن بعد للقمر الصناعي لاندسات ٨

***ضياء أسامة الأنصاري**
معمل الزراعة المنضبطة – قسم الفاكهة – كلية الزراعة (الشاطبي) – جامعة الاسكندرية – الاسكندرية – ٢١٥٤٥ - مصر
*** الباحث المتصل: diaa.elansary@alexu.edu.eg / diaaagri@hotmail.com / Tel.: +02-01000150804**

في هذا البحث، تم استخدام بيانات الإستشعار عن بعد للقمر الصناعي والقياسات الحقلية لبيانات التوثيق الارضي للتعرف على البصمة الطيفية وتقدير مساحة السطح المنزرعة بمحاصيل الفاكهة في منطقة طيبة الواقعة في غرب دلتا النيل في مصر. تم تجميع ببانات نظام تحديد المكان العالمي (GPS) واخذ عينات التربة السطحية الجرداء في منطقة طيبة خلال موسمي ٢٠١٢ و٢٠١٣ م. ولقد أشتملت بيانات التوثيق الأرضي على ١١ محصول فاكهة: البرتقال، اليوسفي، الليمون البنزهير والأضاليا، العنب، التفاح، الخوخ، المشمش، البرقوق، الجوافه، المانجو، والتين الشوكي، و٦ محاصيل اخرى: الطماطم، الكوسة، القمح، البرسيم المصري، الفول البلدي، و بنجر السكر، واخيراً اشتملت على التربة الجرداء. تم استخدام صورة واحدة للقمر الصناعي الأمريكي لاندسات ٨ (Landsat-8 OLI TIRS) تغطي منطقة الدراسة (WRS-path 177 and WRS-row 39) ، تم تصويرها يوم ١٩ مارس ٢٠١٣م، هذه الصورة تم إجراء المعايرة الإشعاعية عليها لتحويلها إلى قيم إنعكاسية ثم تم إنتاج منحنيات البصمة الطيفية لكل نوع نباتي منفرد أو في مجموعات بالنسبة للتربة الجرداء. هذا ولقد تم حساب تسعة دلائل نباتية من الطول الموجي الإنعكاسي للأطوال الموجية الواقعة في منطقة الضوء المرئي والتحت حمراء القريبة والتحت حمراء ذات الأطوال الموجية القصيرة من الطيف الإشعاعي ولقد أشتملت على: دليل تسوية الإختلافات النباتية (NDVI)، دليل النسبة النباتية (RVI)، دليل التحول النباتي (TVI)، دليل الرماد المحترق النباتي (AVI)، دليل ضبط التربة النباتي (SAVI)، الدليل المعدل لضبط التربة النباتي الثاني (MSAVI2)، دليل التاسلت كاب للسطوع (TCB)، دليل التاسلت كاب للإخضرار (TCG)، ودليل التاسلت كاب للإبتلالية (TCW). ولقد تم إجراء تقسيم لإنعاكسية قنوات القمر الصناعي وكذلك للدلائل النباتية لتقدير المساحات المنزرعة بمحاصيل الفاكهة والمحاصيل الاخرى والتربة الجرداء، كما تم تقييم دقة الطريقة البحثية التي تم تطويرها للتقسيم المستخدم. بالإضافة لذلك، تم حساب معادلات نمذجة الإنحدار الخطي المتعدد للتنبؤ بقيم كربونات الكالسيوم (٪) والأملاح الذائبة (ديسيسيمنز/ م)، ورقم الحموضة وقوام التربة (٪ الرمل، السلت، والطين) بإستخدام بيانات الإستشعار عن بعد للقمر الصناعي لاندسات ٨ للقنوات الثمانية الاولى والخاصة بالتربة الجرداء كمدخلات إنحدار، كما تم عرض خرائط التنبؤ بالنظم المعلوماتية الجغرافية (GIS) لوحدات خرائط التربة (SMU) في منطقة طيبة. ولقد أشارات النتائج إلى أن تقديرات المساحة المنزرعة بإستخدام إنعكاسية قنوات القمر الصناعي كانت أكثر دقة من الدلائل النباتية، ويوصى بإستخدام القنوات أرقام ٣ (٠.٥٣ – ٠.٥٩ ميكروميتر) أو ٤ (٠.٦٤ – ٠.٦٧ ميكروميتر) لتقدير المساحة المنزرعة بمحاصيل الفاكهة. كما أوضحت تنبؤات نمذجة الإنحدارالخطي إلى أنه قد تم التنبؤ بمحتوى التربة الجرداء من كربونات الكالسيوم والأملاح الذائبة وكذلك وحدات خرائط التربة بدقة عالية في معظم أراضي منطقة طيبة.